Article:
Azam, A, Ghanbarzadeh, A, Neville, A et al. (2 more authors) (2019) Modelling tribochemistry in the mixed lubrication regime. Tribology International, 132. pp. 256-274. ISSN 0301-679X

https://doi.org/10.1016/j.triboint.2018.12.024

Modelling tribochemistry in the mixed lubrication regime

Abdullah Azam, Ali Ghanbarzadeh,
Anne Neville, Ardian Morina, Mark C.T. Wilson

Institute of Functional Surfaces,
School of Mechanical Engineering, University of Leeds, Leeds, UK

Abstract

Mixed lubrication is a contact condition when the total load is carried by both the fluid lubricant and the solid contacting asperities. The aim of this study is to couple tribochemistry with lubrication. A recent semi-deterministic tribochemical model of tribofilm growth is integrated in a deterministic mixed lubrication model. The model considers the variable hardness of the tribofilm and enables the study of lubrication and tribochemistry and their mutual interaction. Results from the current model are compared against the previously published results. The model can be easily adapted to actual experimental conditions and geometries. The model can be used beyond pure boundary lubrication conditions to monitor tribofilm growth under mixed lubrication conditions.

Keywords: `mixed lubrication, tribochemistry, tribofilm, antiwear, roughness.`

1. Introduction

Lubricants perform various important roles in the operation of machine elements, especially in extreme working conditions. They can reduce friction and wear as well as sustain the loads and assist in cooling the contacting surfaces[1]. This unique set of properties is achieved by enhancing base oil with various additives to increase the efficacy of the system. This improves reliability by increasing the life of components. The underlying mechanism essentially involves tribochemical reactions between the base material and the lubricant additives resulting in the formation of tribofilms. Under mixed lubrication conditions, the presence of localized high shear results in the initiation of these chemical interactions to form tribofilms that protect the system against friction, wear and oxidation [2, 3].

Mixed lubrication models are receiving increasing attention in the tribology community. The science of lubrication is the key to the operation and optimization of almost all power transmission components. The presence of surface roughness on real engineering surfaces results in discrete contact spots inside the nominal contact zone and part of the load is carried by the lubricant and the rest by the solid contacting asperities. This state of lubrication is called *Mixed Lubrication*. The local contact pressures can reach the plastic limit of the material and cause severe shearing of the lubricant films and solid surfaces. These extreme conditions caused by the rubbing of surfaces and shear results in chemical reactions forming chemically adsorbed layers [4, 5].

The mixed lubrication regime is the condition that occurs during the operation of components where the effects of surface roughness dominate the contact performance [6]. In the mixed lubrication regime both elastohydrodynamic lubrication and boundary lubrication regions coexist [7]. The mixed lubrication models require the definition of roughness on the surfaces. If the surface roughness is represented by statistical parameters, the models are *Stochastic* [8, 9]. The load compliance condition given by Greenwood and Tripp [10] is employed. If the surface roughness is defined deterministically, as a matrix of numbers with asperity heights, the models are *deterministic* [11, 12]. Jiang et al. [11] solved the mixed lubrication problem using the separate approach (solving different equations for the solid and lubricated parts) while Hu and Zhu [12] introduced the unified approach (the same Reynolds equation solves pressures in both contact and lubricated regions).

Zinc dialkyl dithiophosphate (ZDDP) is the most successful antiwear additive in lubricants [2]. It controls wear by forming protective tribofilms on the contacting asperities and by digesting abrasive iron oxides particles [13]. The ZDDP tribofilm contains glassy amorphous phosphates [14, 15]. ZDDP can form thermal films [16] as well as tribofilms. The tribofilms are formed due to rubbing and shear and form much quicker and at quite low temperatures ($\approx 25^oC$) [16, 17] compared to thermal films. Both thermal and tribofilms have similar composition [18] and form not only on ferrous substrates but also on ceramics [19, 20], silicon [21] and diamond like carbon (DLC) coatings [22]. The tribofilm mean thickness can reach up to 200 nm [23].

The tribofilms form on the surface inside the rubbing track by several mechanisms like the flash temperatures rise, pressure, triboemission and surface catalysis [24]. The flash temperature is the rapid rise in temperature at the contacting asperities and is thought to be responsible for the ZDDP tribofilm growth [25]. The flash temperature rises significantly at higher speeds but at lower speeds these are negligible. Mosey et al. [26] suggested that the

tribofilm growth is due to the pressure induced cross-linking of the phosphate network. They performed a parametric study but the pressures used were in the range of several gigapascals which were not practical. The presence of roughness inside the contact may create pressures that are high enough to cause plastic deformation. The plastic deformation generates charged regions which emit energetic particles like photons, ions, electrons [27] and X-rays [28]. This triboemission has also been suggested as one of the causes of tribofilm formation [29].

The formation of ZDDP tribofilms or in general tribofilms is considered a stress-promoted thermal activitation process [24, 30]. According to this theory, the effective activation energy for the forward reaction is reduced due to the applied shear stress. The mechanical work adds to the thermal energy to increase forward reaction by lowering the activation energy [31].

The inclusion of tribochemistry in mixed lubrication models is a fairly new concept. Several attempts have been made at modelling the tribofilm growth as a stress-assisted thermal activation process. Andersson et al. [32] developed a model to simulate tribofilm growth and combined it with a boundary lubrication solver to simulate tribofilm growth on real rough surfaces. The tribofilm growth was modelled as a chemical reaction happening due to frictional heating. An Arrhenius type equation was fitted to experimental data and used in the simulation but only short term tribofilm growth was simulated. Gosvami et al. [21] did AFM experiments on silicon substrate to see the effect of pressure and temperature. Their results for tribofilm growth showed a good fit to the stress-dependent kinetic growth model. This model was used by Akchurin and Bosman [33] to predict tribofilm growth and wear using a boundary element based contact model. Ghanbarzadeh et al. [34] developed a similar model based upon the thermodynamics of interfaces. The effect of shear was included by using a multiplication factor called x_{tribo}. They combined their model with a boundary lubrication solver and predicted tribofilm growth and wear in a ZDDP lubricant [35]. Zhang and Spikes [24] have recently reiterated the concept of stress-promoted growth of tribofilm. They conducted experiments with high viscosity fluids and low speeds to see the tribofilm growth in full elastohydrodynamic lubrication film conditions. This study successfully proved the concept of stress-assisted growth of tribofilm. The stress-activated tribofilm growth model given by Zhang and Spikes was implemented into a mixed lubrication solver by Brizmer et al. [36]. This was the first attempt that considered tribochemistry in a mixed lubrication solver. However, although their model included general wear of the system, it did not consider tribofilm formation and removal explicitly as separate contributions to the overall tribofilm and wear dynamics.

Therefore, mixed lubrication models able to capture tribochemistry are

in high demand. In this study a unified mixed lubrication model is developed where the complete pressure profile is obtained by solving the Reynolds equation alone. This mixed lubrication model is combined with the tribofilm growth model from Ghanbarzadeh et al. [34]. Their model requires some parameters to be fitted to experimental tribofilm growth results and combines the effect of flash temperatures with shear through the factor x_{tribo}. The parameter fitting values are adopted from their work and used as such in the current study to simulate tribofilm growth. The term x_{tribo} is directly related to shear at the interface and the kinetics of tribofilm growth. The increase in shear stress is directly reflected by the higher values of x_{tribo} as shown in reference [35]. Moreover, the parameter x_{tribo} is also sensitive to the lubricant chemistry and concentration as well as the temperature of the system [37]. The wear in this work is modelled by modifying the Archard wear equation to include the effect of tribofilm growth. More details on the tribofilm growth and the wear models are presented in section 2.3 to 2.5.

This study presents the tribofilm growth on the surfaces and the mean values of tribofilm thickness as a function of time. The wear evolution is also presented. The tribofilm and wear measurements are compared against published simulation results. The tribofilm growth and wear can be simulated within the unified mixed lubrication framework. The integration of the tribofilm growth, wear and plastic deformation within the mixed lubrication algorithm enables the simulation to be performed irrespective of the computational node being under fluid or solid contact condition. Moreover, the deformation can be elastic or plastic and may be caused by solid or fluid pressures. The resulting tribochemical mixed lubrication framework provides a highly valuable tool. The model is also capable of simulating the entire wear track profile evolution with time, and is flexible enough to be applied to various tribological systems and experimental configurations. The present model can predict tribofilm formation in both the boundary and mixed lubrication conditions, and potential applications are illustrated.

2. Model components

In this paper, the contact between a rough spherical ball and rough disc is simulated as an illustration of the model. Rough surfaces are generated using in-house code which is based upon the method of Tonder et al [38]. The model is also capable of reading the real rough surface topography as numerical inputs. Both the macro- and micro-geometries are considered in this contact. The contact between the two rough surfaces is solved to get the contact pressures and film thickness distribution inside the contact. In the following sections, the model components are discussed. First a brief account

of the unified mixed lubrication model is given, then the tribochemical film growth model is outlined. The next section outlines the numerical procedure, specifically highlighting the integration of these two models and the solution procedure.

2.1. Mixed lubrication model

The complete pressure distribution is governed and computed by solving the Reynolds equation, given as

$$\frac{\partial}{\partial x}\left[\left(\frac{\rho h^3}{12\eta}\right)\frac{\partial p}{\partial x}\right]+\frac{\partial}{\partial y}\left[\left(\frac{\rho h^3}{12\eta}\right)\frac{\partial p}{\partial y}\right]=\left(\frac{u_1+u_2}{2}\right)\frac{\partial(\rho h)}{\partial x}+\frac{\partial(\rho h)}{\partial t} \tag{1}$$

where h is the film thickness, p is the pressure, u_1 and u_2 are the surface velocities for the ball and disc, ρ and η define density and viscosity of the lubricant and x and y denote the coordinate directions. The lubricant properties are described through its viscosity. In this study the lubricant is assumed Newtonian and the x-coordinate is aligned with the flow direction. Two boundary conditions are applied. A boundary condition of $p = 0$ is applied at all the edges of the solution domain and all negative pressures are clipped to zero to implement cavitation boundary condition i.e. $\{\forall\ x \geq x_e,\ p < 0 \Rightarrow p = 0\}$.

The mathematical nature of the Reynolds equation, equation 1, is such that under extreme contact conditions of high load and low speed when the film thickness approaches zero, the terms on the left hand side approach zero. The conventional solvers based upon the Jacobi and Gauss-Seidel methods fail under such conditions. Thus, if the Reynolds solver can be made robust enough to handle this extreme condition, the asperity contact pressures can also be predicted by solving equation 1. Two key changes are made to conventional solvers. First, the coefficient matrix for the discretized Reynolds equation is built with contribution from the entrainment flow terms as well (the terms on the right hand side of equation 1). Second, to avoid computational difficulties in dealing with the very small values close to zero, a criterion is imposed on the film thickness values whereby whenever the local lubricant film thickness value falls below a threshold value (1 nm in the current study), it is considered as a flow obstruction and is considered zero.

The film thickness is also termed as gap as it defines the relative gap between mating surfaces. The film thickness equation for the point contact is expressed as

$$h = h_0(t) + \frac{x^2}{2R_x} + \frac{x^2}{2R_y} + v_e(x, y, t) + \delta(x, y, t) \tag{2}$$

where h is the film thickness, h_0 is the undeformed gap, R_x and R_y are the radius of curvature in the x and y direction and the term $\frac{x^2}{2R_x}+\frac{x^2}{2R_y}$ defines the macrogeometry of the contact. The term $\delta(x, y, t)$ is the roughness function and this defines the microgeometry of the contact. The term v_e describes the total deformation which may be elastic or plastic. The algorithm applied here limits the pressures in successive iterations. The magnitude of plastically deformation is then taken out of the total deformation to create a permanent change in the geometry of the contacting pair. The surface elastic deformation is represented by the Boussinesq integral formulation formulation.

$$v_e = \frac{2}{\pi E'} \int \int_\sigma \frac{p(x, y)}{\sqrt{(x' - x)^2 + (y' - y)^2}} dxdy$$

where p is the pressure, x and y are the coordinate directions. The prime on x and y denote the point of application of pressure while the non-primed x and y correspond to the point of calculation as the pressure applied at a point influences other points as well. The Boussinesq equation gives the deformation on a continuous half space. To solve this equation numerically, it has to be converted into discrete form by assuming a piecewise constant distribution of pressure leading to discrete pressures, p_{kl}, at the computational nodes. The integral then takes the form of a deformation matrix:

$$V_{ij} = 2\frac{\Delta x}{\pi^2} \sum_{k=1}^{M} \sum_{l=1}^{N} D_{ij}^{kl} p_{kl}$$

In this equation, p defines pressure, Δx is the grid size, the matrix D_{ij}^{kl} is called the flexibility matrix. This matrix forms a convolution with pressure which can be solved more efficiently using Fast Fourier Transforms (FFTs). The use of FFTs makes the solution process quicker and makes denser grids accessible.The deformation matrix is written as convolution

$$V(X_i, Y_j) = \sum_{k=1}^{M-1} K(X_i - X_k, Y_j - Y_k) * P(X_k, Y_k)$$

The application of FFTs requires the conversion of this linear convolution to a cyclic convolution and by pre-treating the pressure matrix and the flexibility matrix [39]. The DC-FFT method is computationally more efficient compared to other methods for calculation of surface deformation [40]. The viscosity is considered as a function of pressure and the Roelands equation [41] has been used in this study to describe it:

$$\eta(p) = \exp\left(\ln(\eta_0) + 9.67\right)(-1 + (1 + \frac{P_H}{p_0} p)^z) \tag{3}$$

The term η_0 is the viscosity at ambient conditions and z is a dimensionless parameter called Roelands pressure viscosity index obtained through curve fitting. In the current study, z=0.68 was used. The term η_0 is the viscosity at ambient pressure and the pressure $p_0 = 1.96 \times 10^8$ Pa is a constant value. The lubricant density is also considered a function of pressure and is calculated using the following equation given by Dowson and Higginson [42],

$$\rho = \rho_0 \big(1 + \frac{0.6 \times 10^{-9} p}{1 + 1.7 \times 10^{-9} p}\big) \tag{4}$$

where ρ_0 is the density at atmospheric pressure. The final equation is the load balance equation which ensures that the applied load is balanced by the pressures. The load balance equation for the point contact is given as

$$w - \int_{y_a}^{y_b} \int_{x_a}^{x_b} p(x, y) dx dy = 0 \tag{5}$$

where a, b, c, d represent the boundaries of the solution domain and w and p are the the applied load and the resulting pressure respectively. The load balance condition imposes a very important physical constraint on the pressure solution. The pressure and film thickness profiles will converge even without the application of load balance condition but the pressure distribution may not be physically right. The inclusion of load balance equation ensures that the calculated pressures are the true physical pressures.

These Equations (1) to (5) form a complete set which is solved to obtain the mixed lubrication pressure and film thickness profiles. The solution requires a robust numerical procedure as the equations are highly non-linear in character. An iterative process is applied, which starts with an initial guess given by a Hertzian pressure profile. This pressure is used to calculate the film thickness which is again used to update the coefficients in the Reynolds equation and pressures are updated. This successive update of pressure and film thickness continues until the desired accuracy is achieved. In this update procedure, the load balance condition is applied to update the undeformed gap in the film thickness equation 2.

The numerical procedure for the solution of the mixed lubrication is based upon the tridiagonal matrix algorithm (TDMA). The Reynolds equation is first discretized using finite differencing technique. The pressure flow terms (left hand side of equation 1) are discretized using the central difference approach and the entrainment flow terms (right hand side of equation 1) are discretized using first order backward differences. The problem is then formulated as a linear algebra problem $AY = B$ where A is the coefficient matrix. It is of the order $N \times N$ and in the current study it is built from the

pressure flow as well as the entrainment flow terms. The vector Y contains the unknown values. For a line contact problem only one system of equations $AY = B$ is solved but for a point contact problem, a series of systems of equations is solved. A direct iterative approach is utilized to solve the problem. The flexibility of the iterative solvers is coupled with the accuracy of the direct solvers. The relaxation factor used is 0.2 which means that 20 % of the new values are used in successive steps within the iteration. The convergence criteria for the pressure convergence loop was fixed between 5×10^{-5} and 5×10^{-4} while the convergence criteria for the load balance condition was fixed at 1×10^{-4}. During an iteration, the pressure predicted by the Reynolds solver is used to update the flexibility matrix which is then used again to update the coefficient matrix for the Reynolds solver. This procedure is repeated until converged pressure and film thickness values have been obtained. In the current study, the difference in the film thickness values was found to be less than 1 % when the mesh density was changed from 128 x 128 to 256 x 256. Therefore, a mesh density of 128 x 128 is employed. Liu et al. [43] also suggest that this mesh density is sufficient to get accurate results.

2.2. Plastic deformation modelling

The plastic deformation model developed in this work is based upon the idea that the nodes that deform plastically float on the surface to form a plane. The criterion for plastic deformation is assumed to be the condition where the pressure at a node reaches the average yielding pressure (hardness of material). Once a node is under plastic deformation, the pressure on this node is limited to the yielding pressure. It is due to this condition that more nodes start to support load and the contact area increases. The yielding pressure is generally found to be 2.8 times the yield strength [44]. The plastically deforming nodes eventually form a plane. Sahlin et al [45] used similar concept to develop an elastic-perfectly plastic model under mixed lubrication. Their model is based upon the assumption of dry contact which requires the application of complementarity condition and is not a true plastoelastohydrodynamic lubrication (PEHL) model.

The PEHL model applied in the current study is based upon the recent publication by the present authors [46]. The application of this elasto-plastic deformation algorithm requires modifications to be made to the Reynolds solver. The first change is made within the solver, at the point of application of load balance condition. The points that undergo yielding are considered to float i.e. no further load can be supported by these nodes unless the pressure at these nodes falls below the average yielding pressure value. The load at these nodes is limited to the yielding pressure. This is achieved

by limiting the pressure values during the summation in equation 5 to the yielding pressure i.e. $\forall P \geq P_y, P = P_y$ while calculating the undeformed film thickness value, h_o in equation 2. This modifies the film thickness values to account for the elasto-plastic contact behaviour. This process gets repeated as it is a part of the pressure and film thickness convergence loops. No other modification is required inside the Reynolds solver.

Once the pressure and film thickness have converged, the nodal pressures are truncated and the reduced elastic deformation is calculated using these truncated pressures. The plastic deformation is evaluated by subtracting this new film thickness for all the plastically deforming nodes from the minimum value of the new film thickness among the elastically deforming nodes. The truncated pressure is then given as initial guess to the EHL solver and the Reynolds solver is again used to get the new pressure profile and film thickness. In this way, by repeating this process, the solution moves from purely elastic to elasto-plastic until a converged is achieved. More details on the method can be found in [46] and [47].

2.3. Tribochemistry modelling

The frictional energy at the contact due to localized shear stress causes chemical reactions to form tribochemical layers at the contacting interface. As mentioned, several attempts have been made in the past to capture this mechanochemical phenomenon [32, 34, 33, 36]. The tribofilm growth model of Ghanbarzadeh et al [34] is adopted in this study to simulate this interfacial tribochemical phenomenon. This model considers the effect of flash temperature and the mechanochemical action and assumes the tribofilm growth phenomenon as a chemical reaction between the lubricant additives and the substrate. The tribochemical reaction rate was introduced based on the work of Balgarevich et al. [48, 49] which highlighted the importance of mechanical rubbing in the tribochemical action. The tribofilm model considers formation of tribolayers due to thermal as well as mechanical stimuli. An Arrheneius type equation captures the thermal growth of the tribofilm and multiplication of the rate coefficient by a parameter, x_{tribo} captures the increase in growth rate due to mechanoactivation. With some mathematical simplifications and assuming a second order chemical reaction, the final equation to express the tribochemical film growth was given as:

$$h = h_{max} - h_{max} e^{(-\frac{k_1 T}{h'})x_{tribo} t} \tag{6}$$

where k_1 and h' are the Boltzmann's and Planck's constants while T and t are the asperity flash temperature and time, respectively. Using this equation, the local tribofilm growth can be simulated. The assumption of a second

order reaction might not be true as in reality multiple chemical reactions are occurring at the interface. This makes it very difficult to guess the true order of the tribochemical reactions. However, this simplified approach is a good initial approximation. In equation 6, the parameters h_{max} and x_{tribo} are fitting parameters which are fitted to experimental data for one loading case. Once the fitting procedure is complete, the fitted equation can be used to simulate tribofilm growth under various conditions. The temperature used in this equation is the asperity flash temperature plus the bulk temperature. The flash temperature is calculated using the slightly modified form of the Jaeger's moving heat source analysis as given in [50].

The tribofilm removal is an important part of the model. It was assumed that the tribofilm formation and removal takes place simultaneously. The tribofilm grows on the substrate due to this competing phenomenon of formation and removal of the tribofilm. This assumption is reasonable and has been reported in other studies as well [51, 52]. The introduction of the removal term in this work enables the comparative study of the tribofilm removal and the wear of the system. The authors [34] used an exponential function to simulate the removal of the tribofilm due to the fact that this function can capture wide range of features of the tribofilm behaviour. Thus, adding the removal part to equation 6 gives

$$h = h_{max}\big(1 - e^{(-\frac{k_1 T}{h'})x_{tribo}t}\big) - C_3\big(1 - e^{-c_4 t}\big) \tag{7}$$

The constants C_3 and C_4 are also fitting parameters. Their values are obtained from experimental fitting.

The tribofilm growth model in equation 7 mainly calculates the growth of tribofilm as a dynamic balance between formation and removal of tribofilm but not the wear of the substrate.

2.4. Mechanical properties of the tribofilm

The tribofilm has different mechanical properties compared to the substrate, and several studies have focussed on the assessment of these properties [53, 54, 55, 3, 56]. These studies suggest that the tribofilm hardness depend upon applied loads and are different at the surface compared to near the bulk substrate. To account for this variable hardness, the approach presented by Andersson et al. [32] has been used in the current work. The tribofilm hardness near the bulk substrate is assumed to be 6 GPa, which is assumed to be the hardness of the substrate. When the tribofilm has its maximum thickness value, the hardness is assumed to be 2 GPa. This was first implemented by Andersson et al. [32] and then used by Ghanbarzadeh et al. [34]. The key idea is to have the hardness varying with the thickness of the tribofilm as the

tribofilm builds up. The change in hardness on the local scale also changes the plastic behaviour. This change in plasticity is included by varying the hardness at the local scale.

2.5. Wear modelling

A modified version of the Archard's wear equation [57] is used in the present work. The pressures at the asperity contacts are used to estimate wear. The mixed lubrication solver is used to calculate pressures and then directly used in the wear equation to calculate the depth of wear at an instant. The nodal pressures are kept constant during each time step for wear and tribofilm calculation. Archard's equation is implemented in the form that it directly gives the localized wear depth.

$$\Delta h(x,y) = \frac{K_{tr}}{H} p(x,y) v \Delta t \tag{8}$$

where K_{tr},H and v are dimensionless wear coefficient, hardness of the substrate and the sliding speed, respectively. The term $p(x,y)$ is the local discrete pressure. The wear coefficient is evaluated experimentally. In this work it is assumed, as in [34], that the coefficient of wear is reducing linearly with the increase in film thickness.

$$K_{tr} = K_{max} - (K_{max} - K_{min}) \frac{h}{h_{max}} \tag{9}$$

In the current study, $K_{max} = 10^{-5}$ and $K_{min} = 10^{-6}$. This formulation of the wear coefficient enables the simulation of antiwear and extreme pressure characteristics of the tribofilm. It is to be noted that the wear modelled in this work is the mild wear and it considers the loss of substrate material due to reaction with the lubricant additives. It was argued in the original model development study [34] that this equation 7 is valid when ZDDP or other phosphorous containing antiwear additives are used with steel substrate and does not necessarily predict the tribochemical film growth behaviour in the presence of other additives or substrates.

It is important to note that the growth of tribofilm and wear in the presence of tribofilm are two independent parameters. Several experimental [58] and theoretical [59, 34] studies show that the concentration of the substrate atoms decreases towards the top of the tribofilm produced by ZDDP on steel. The detachment of material from the surface due to contact results in the removal of substrate atoms as well. This reduced concentration of the substrate atoms from substrate to the top of the tribofilm supports the fact that less wear of the tribofilm occurs when tribofilm is thick. The wear of

substrate is calculated using equation 8 where as the removal part in equation 7 is a phenomenological mathematical model to capture the dynamic growth behaviour of tribofilm. This wear is mild wear of the substrate in the presence of tribofilm.

3. Numerical implementation details

In this study it is assumed that the tribofilm only forms at the contacting asperities. Some recent studies have suggested that the tribofilm growth is a shear induced mechanochemical activation phenomenon [24]. As mentioned in the introduction section 1, the growth of tribofilm occurs by various mechanisms, flash temperature rise, pressure, triboemission and surface catalysis and stress inside the rubbing contact. Different mechanisms are active under different lubrication conditions. The simulation results presented in this work are for contact conditions that are near to the boundary lubrication regime where the flash temperature, pressure and shear are dominant at the contacting asperities. Thus, the tribofilm growth model selected in the current study is the right choice as it takes into account both the thermal and shear induced tribofilm growth.

The mixed lubrication model calculates the contact pressures and film thickness profiles based upon the rough surface contact as explained in section 2.1. These pressures are used to calculate the tribofilm growth and wear which are used to modify the corresponding geometry of ball and disc. The geometries for the next iteration have been changed by plastic deformation, wear and the localized tribofilm growth. The wear modelled is the mild wear, and only alters the geometry of the substrate and not the tribofilm. The tribofilm removal is considered as independent from wear. Figure 1 gives a flow chart of the numerical procedure. The mixed lubrication equations are solved in the non-dimensional form and correspond to a square area of approx. 0.5 mm by 0.5 mm. For the tribofilm growth and removal, the calibrated values from the work of Ghanbarzadeh et al [34] are used and are given in table 1.

For all the simulation cases presented in this paper, the material yield limit is fixed at 6 GPa for the substrate and 2 GPa for the tribofilm of maximum thickness. The applied load is fixed at 60 N, the equivalent radius of ball R_x is 10 mm and the disc radius is taken as 39 mm (SKF bearing washer WS 81212). The entrainment speed is fixed at 0.25 m/s. The slide to roll ratio (SRR) is varied from 0% to +10%. A Newtonian lubricant with viscosity $\eta = 0.004$ Pa.s and a pressure viscosity coefficient $\alpha = 14.94$ GPa^{-1} is lubricating the contact. The equivalent Young's modulus for the interface is $E = 230.47$ GPa. The temperature in our simulations is fixed

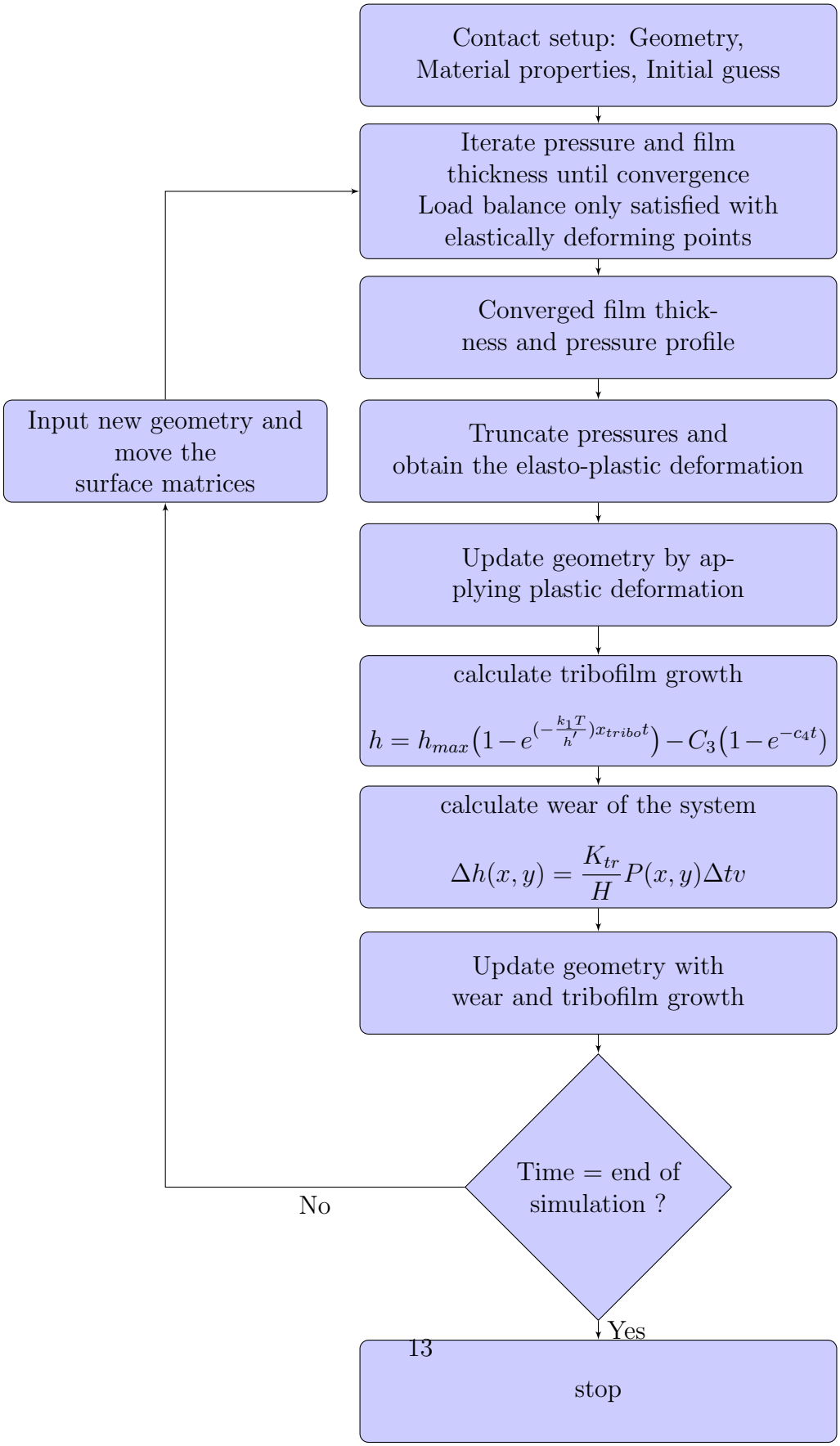

Figure 1: Flow chart to explain the numerical procedure

Parameter	Symbol	Value
Steel wear coefficient (dimensionless)	K_{max}	10^{-5}
Maximum tribofilm wear coefficient (dimensionless)	K_{min}	10^{-6}
Maximum local tribofilm thickness	h_{max}	$176nm$
Tribofilm formation rate constant	x_{tribo}	4.13×10^{-16}
Tribofilm removal constant	C_1	112.5 nm
Tribofilm removal exponential factor	C_2	0.0006799

Table 1: Parameters calibrated from experiments [34]

at 90^{o}C unless otherwise stated. The Reynolds equation is solved in steady state form and the transient terms are turned zero. This is because the time steps involved in the Reynolds solver are too small to have any significant tribofilm growth. So, the Reynolds equation is solved quasi-statically and the time step is chosen based upon the loading cycles and is much greater than the time step of the Reynolds equation. This enables simulations to be performed on realistic time scales.

4. Results and Discussion

The tribopair in the simulation set up is formed by a disc of radius 39 mm and roughness 100 nm sliding against a ball of radius 10 mm and roughness 10 nm. The positive slide to roll ratios correspond to the faster surface speeds of the ball. The results are presented for four representative slide to roll ratios.

4.1. Tribofilm growth

The instantaneous tribofilm growth will be discussed in this section. The experimental observations [21] suggest that the tribofilm grows in patchy fashion and is inhomogeneous. A close look at figure 2 shows that the model captures this inhomogeneity and patchiness effectively. The tribofilm growth is plotted at different times through the simulation time scale. It can be seen that the growth of tribofilm starts as patches of tribofilm growing within the rubbing track. These patches then keep growing along the direction of flow in an inhomogeneous manner. The inhomogeniety is linked to the roughness of the surface. When rough surfaces come into contact a mixed contact is formed with discrete solid and fluid lubricated regions. The asperities carry greater load and undergo higher shear. Thus, more film growth takes place at these high shear points on the surface and the film formation and removal rates vary as well. This eventually gives rise to the inhomogeneous tribofilm growth pattern. Not only the thickness of the tribofilm but the

coverage is also inhomogeneous. The dynamic evolution of the contact due to plastic deformation, wear and tribofilm growth results in the flattening of the asperities which in turn increases the real area of contact leading to increase in coverage. Moreover, the growth of tribofilm is greater at high pressure nodes and due to the fact that tribofilm has lower hardness compared to substrate, the shear is less at these nodes. Therefore, the height of asperities is retained at these nodes and this ultimately leads to retaining high pressure at these nodes and tribofilm thickness continues to increase at these high pressure nodes resulting in patchiness. This leads to patchy tribofilm growth. This tribofilm growth behaviour is consistent with experimental observations [2].

The general procedure to obtain experimental tribofilm growth data is by using the spacer layer interferometry method (SLIM) [16]. The tribofilm thickness is approximated by taking the average of the local tribofilm thickness values within an observation window and the mean tribofilm thickness value is reported. Therefore, the averaging procedure used in this study is a valid approach to represent tribofilm growth results. In the simulation set up the tribofilm growth on both the ball and the disc can be observed. The tribofilm grows within the rubbing track. It can be seen that the wear track width increases due to plastic deformation and wear as the simulation progresses. The tribofilm thickness presented in this study is the mean thickness of the tribofilm formed at all the points inside the rubbing track. Figure 3 presents the mean tribofilm growth on the disc surface and figure 4 gives the mean tribofilm growth on the ball surface. The tribofilm growth behaviour on both the ball and disc is similar but the differences observed are due to the differences in the removal and coverage rates of the tribofilm. The rougher surface (disc) tends to form thicker mean tribofilms compared to the smooth counterparts. The results agree well with the results from Ghanbarzadeh et al. [34] but the predicted values of mean tribofilm thickness are slightly smaller as shown in figure 5. This may be because of the effect of lubricant which is present in the current model but absent in their work and a recent study by Spikes et al. [24] has suggested that the lubricant shear can also form tribofilms. Thus, lower values of mean tribofilm thickness are expected. In the work of Ghanbarzadeh et al. [34] no correlation was found in the growth behaviour with change in slide to roll ratio (SRR). The variation of tribofilm growth rate with SRR in this work is consistent with the results given by Andersson et al. [32] as shown in figure 6. Once again the predicted tribofilm mean values are lower but the current study is able to simulate the overshoot which Andersson et al. were not able to produce. The final mean tribofilm thickness value at the end of experiment is spread within a narrow range of values but this is not considered important in experimental

results [60]. In the experiments, it cannot be consistently measured. The model predicts lower mean tribofilm thickness values for higher SRR for the smooth surface while higher mean tribofilm thickness values for higher SRR for the rougher counter part.

The general observations mentioned above show that despite the growth behaviour is similar but due to the large differences in the roughness, the tribofilm grows on the two counterparts differently. The overshoot is clearly visible in the mean tribofilm growth values on the ball which is the smoother counterpart but not on the disc which is the rougher counterpart. This may be linked to the difference in the removal rates of tribofilm on both the surfaces as well as the difference in the coverage of tribofilm on both the surfaces. Another important factor is the mean value of tribofilm which is thicker on the rougher surface while thinner on the smooth surface. On the other hand, the smooth surface reaches full coverage (100%) faster where as the the coverage on the rougher surface takes longer to reach full coverage and sometimes never reaches 100% coverage even at the end of simulation.

4.2. The effect of lambda ratio

One of the key outcome of this study is the integration of tribofilm growth with the mixed lubrication models. Therefore, It is important to illustrate the capability of the model to observe tribofilm growth by varying the severity of contact while staying in the mixed lubrication conditions. Thus, a set of simulations were performed by changing the entrainment speed which changes the lambda ratio. Figure 7 shows the evolution of mean tribofilm thickness values for different values of lambda ratio. The lower the entrainment speed, the lower the lambda ratio and thicker the tribofilm. The lower values of lambda ratio correspond to the greater area supported by the solid contacting asperities and thicker tribofilms are expected. Therefore, the model correctly predicts the tribofilm growth behaviour at different values of lambda ratio. Not only the mean tribofilm thickness values change by varying the lambda ratio but the growth rate also varies as the simulation progresses in time. From figure 7, it can be seen that the rate of increase of tribofilm growth decreases with increasing lambda ratio. The model provides a versatile tool that can be used to optimize lubricant performance and design. Moreover, changing the lubrication regime from full film down to boundary lubrication and vice versa, the corresponding contact characteristics can be predicted and monitored through time. On the other hand the evolution of the lubrication regimes can also be monitored through time by varying the contact performance parameters (speed, load and viscosity etc.).

4.3. Tribochemical Wear

It is assumed in the present study that the tribofilm growth and wear of substrate take place at the asperity contacts only. This assumption is valid as the applied conditions are close to the boundary lubrication regime with little or no effect of lubricant pressure. Thus, the effect of lubricant in causing wear is neglected. The wear results are presented as mean wear depth inside the wear track. The wear presented here is the mild wear which is the wear of the substrate in the presence of tribofilm. The wear depth profiles are given in figure 8 for the disc surface and in figure 9 for the ball surface. The wear depth profiles are the sum of mild wear and plastic deformation. From the wear depth plots, it can be seen that the wear on the ball is considerably higher compared to the wear on the disc. This is because the ball effectively stays in the contact for longer time and thus, undergoes more wear. The wear behaviour correlates well with the mean values of the tribofilm formed on both the disc and ball. On some nodes on the disc, the trbofilm growth is close to zero while on some of the nodes the tribofilm grows very thick. As the disc is almost 10 times rougher than the ball, the load on the disc is mainly carried by asperities. These asperities experience very high loads and stresses and the tribofilm growth on these asperities is also considerably higher. This reduces the wear significantly on these asperities due to the antiwear action. The wear on the ball is quite high. There are various reasons to this. First of all, the ball spends effectively more time inside the contact and thus, undergoes more loading cycles for each loading cycle on the disc. Secondly, the overall low value of mean tribofilm thickness over most of the ball surface results in lowering the wear on the ball but the wear reduction is lower due to thinner tribofilm formed. Thus, overall higher values of wear coefficient prevail over the ball surface. The plastic deformation is only present during the initial 20 to 30 mins and is zero afterwards. The presence of high plastic deformation is responsible for the steeper wear depth profiles during this initial running in period.

The effect of SRR on wear is complicated due to interplay between shear and loading cycles. For two surfaces of similar roughness, the increase in sliding will result in higher wear. But for the contacting surfaces having different roughness as in the current case, it is not only the amount of sliding (shear) that determines wear but the amount of time that a particular surface spends inside the contact as well as the number of times the rougher surface moves through the contact determine wear behaviour. The effect of SRR on the ball surface is clearly identifiable: the higher the SRR, the greater the number of loading cycles for the ball and thus more wear. But for the disc it is not clear whether the increase in SRR increases or decreases wear. From the plots of mean wear depth for the disc, it can be seen that wear rates

are affected by the changes in SRR but the final wear depth reaches similar values for all SRR values. This behaviour of the disc wear can be attributed to the higher value of roughness on the disc compared to the ball.

The current model is capable of giving 3-D wear track profiles. A sample 3-D wear track profile is given in figure 10 for illustration purpose.

5. Conclusion

A mixed lubrication model with tribochemistry was developed and numerically implemented. The implementation details were given and the results were presented for a sample calculation done to validate the model against published tribofilm modelling results [34, 32]. The tribofilm growth results were presented for the ball and the disc and and it was found that the tribofilm grows in patchy, inhomogeneous manner within the rubbing track. The mean tribofilm thickness value was found to increase with increasing SRR value. An increase in lambda ratio was found to decrease the thickness of tribofilm. The wear in the presence of tribofilm was also modelled and the results were plotted as 2-D averaged and 3-D wear track profiles. An increase in SRR was found to give higher mean wear for the smoother surface while the effect of SRR on the rough surface was not clear.

The currently developed model can simulate the tribofilm growth in the mixed lubrication regime and enables the study of lubrication, wear and their interaction. The model enables the study of not only the tribofilm growth but can also be used to see the effect of this film growth on the lubrication performance.

Acknowledgement

The study was funded by the FP7 program through the Marie Curie Initial Training Network (MC-ITN) entitled "FUTUREBET - Formulating an Understanding of Tribocorrosion in ardUous Real Environments - Bearing Emerging Technologies", grant no. 317334 and was carried out at the University of Leeds.

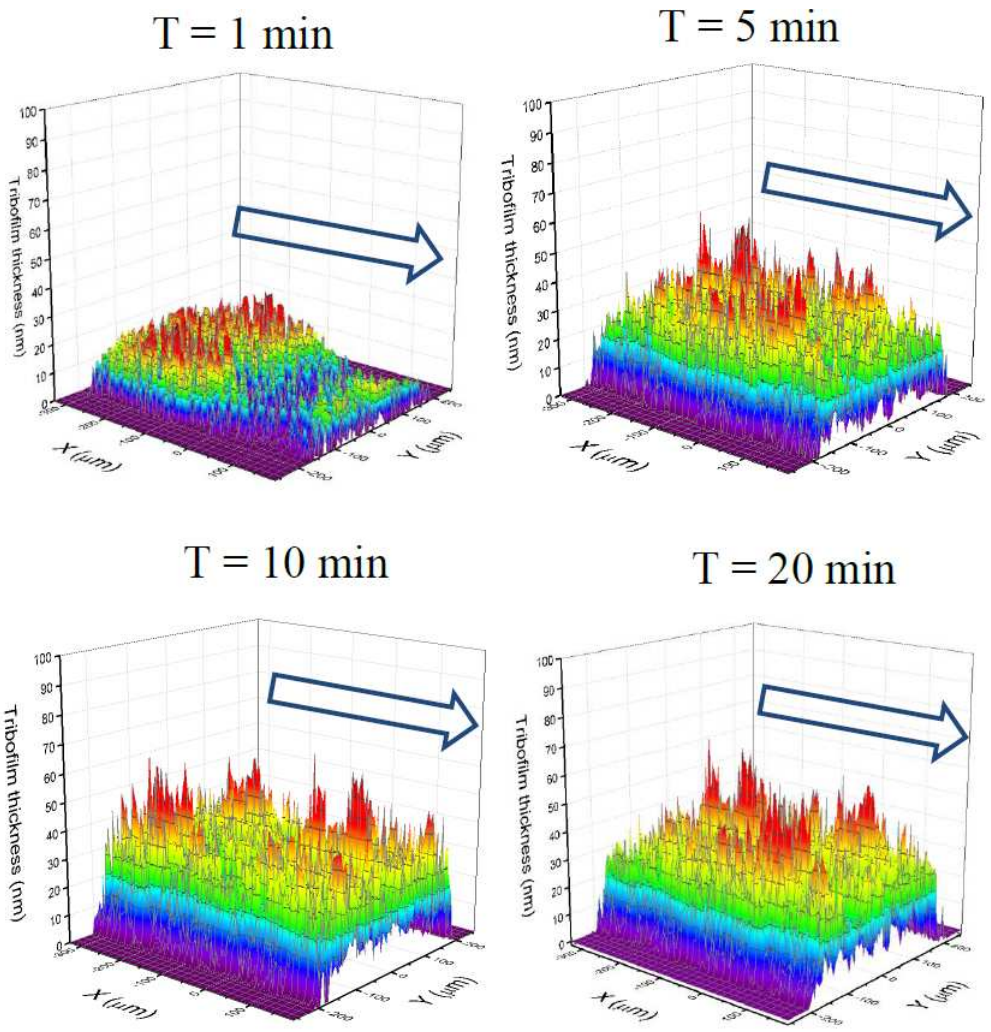

Figure 2: The evolution of tribofilm growth on the smooth counter part with time. The patchy appearance of tribofilm due to inhomogeneous growth of tribofilm

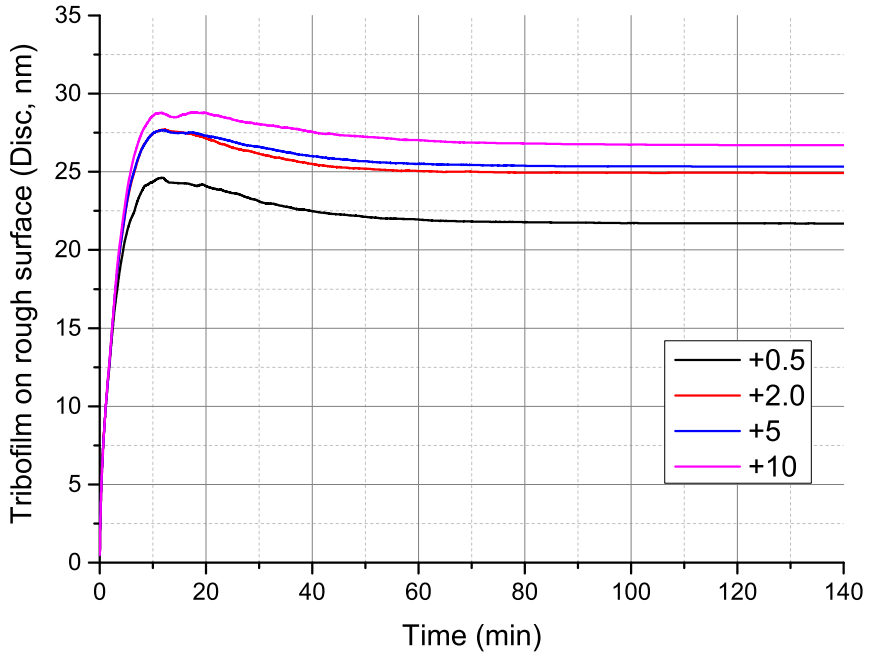

Figure 3: Tribofilm growth on the rougher counter part; Disc (Ra 100 nm, Rq 126 nm) for different SRR. The legend in the figure represent different SRR values as percentage sliding.

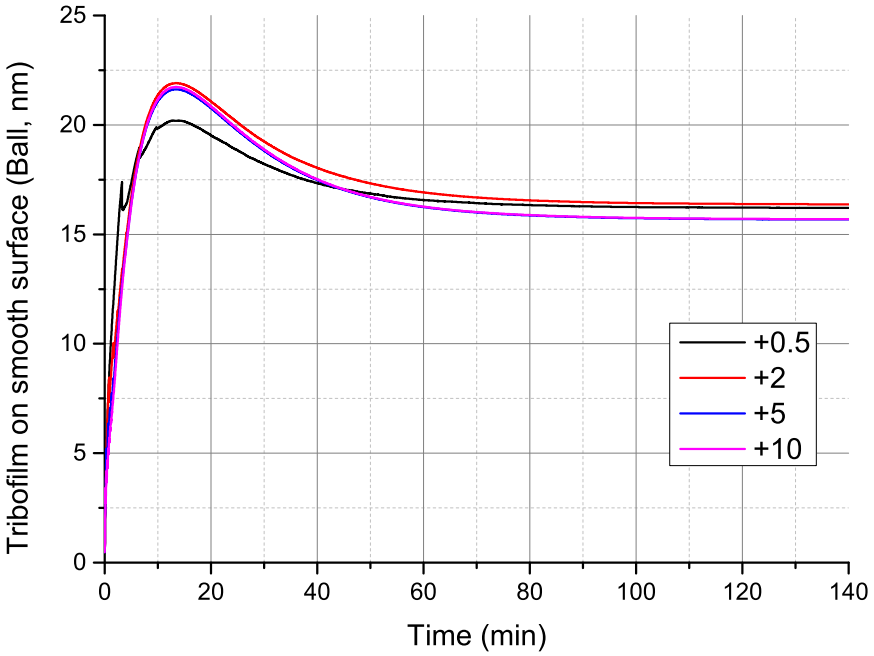

Figure 4: Tribofilm growth on the smoother counter part; Ball (Ra 10 nm, Rq 12 nm) for different SRR. The legend in the figure represent different SRR values as percentage sliding.

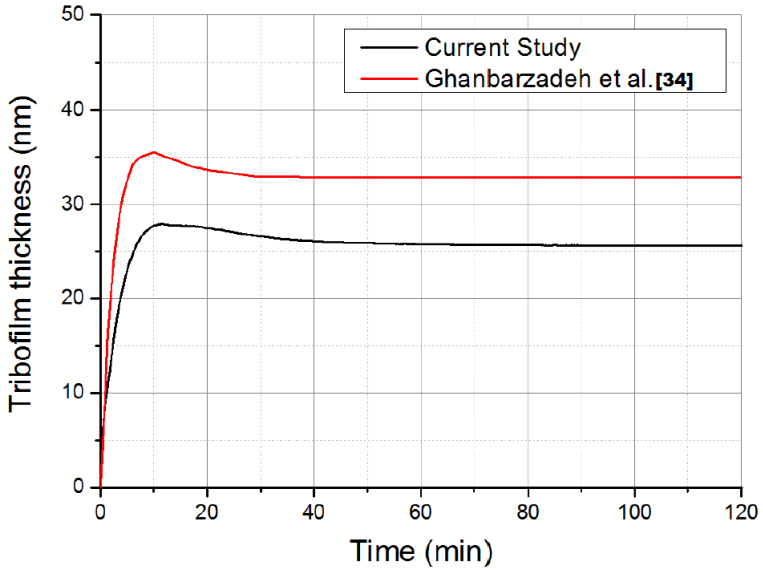

Figure 5: Comparison of tribofilm growth from current model against the work of Ghanbarzadeh et al. [34] for SRR = +2%

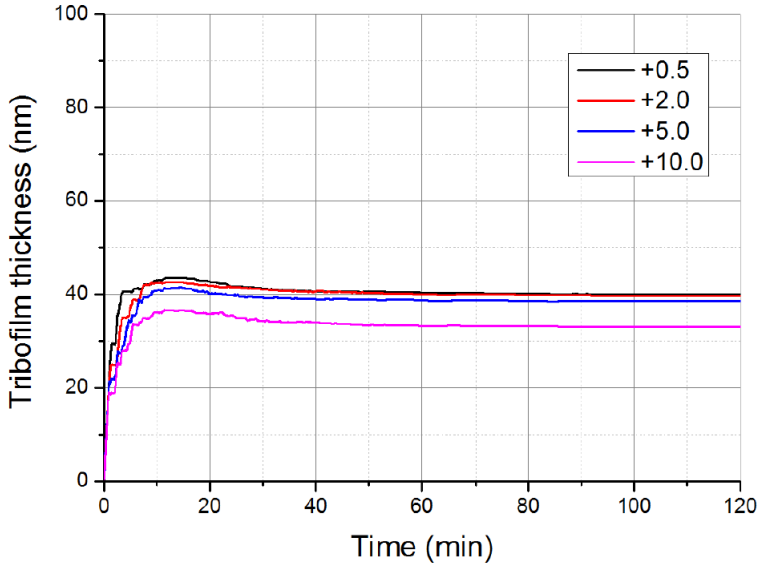

Figure 6: Mean tribofilm thickness values plotted as function of SRR over time. The legend in the figure represent different SRR values as percentage sliding.

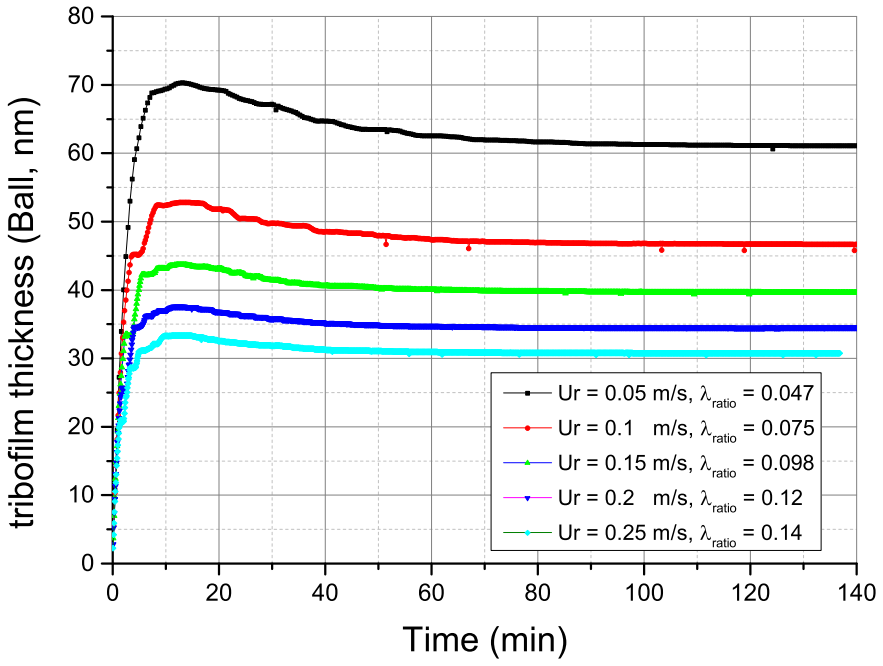

Figure 7: Tribofilm growth under mixed lubrication conditions. Mean tribofilm thickness plotted as a function of lambda ratio.

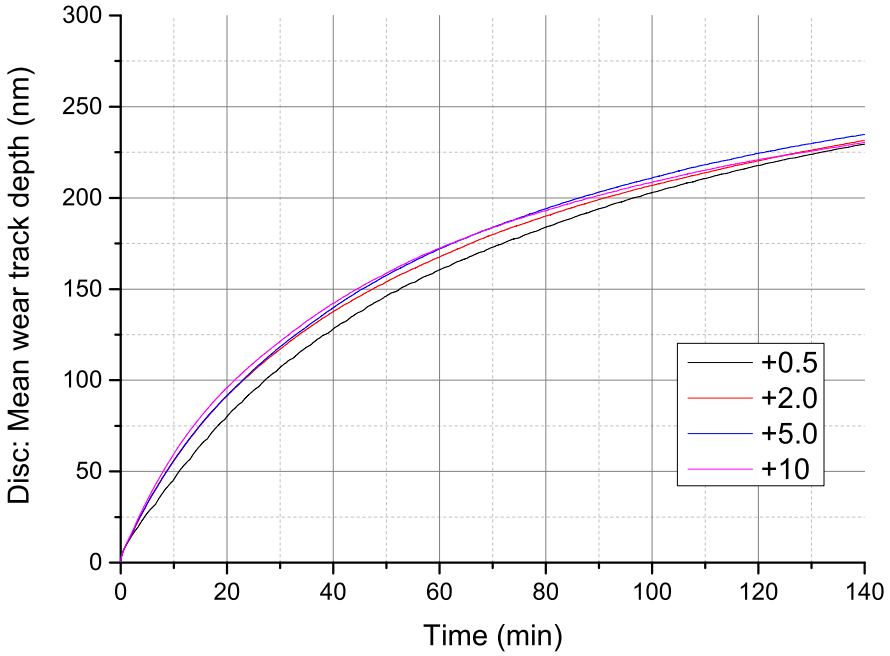

Figure 8: Wear track depth on the rougher counter part; Disc (Ra 100 nm, Rq 126 nm) for different SRR. The legend in the figure represent different SRR values as percentage sliding.

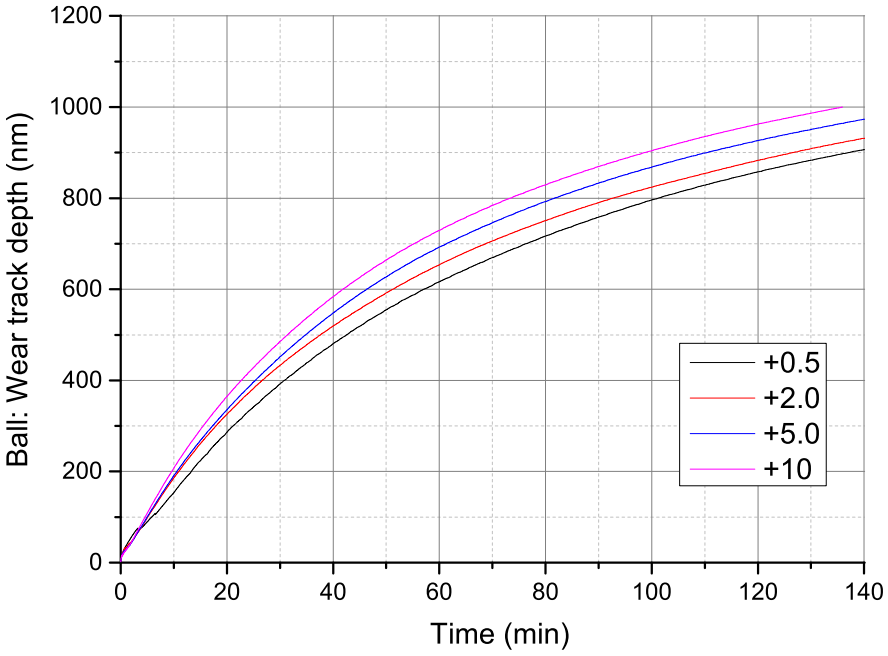

Figure 9: Tribofilm growth on the smoother counter part; Ball (Ra 10 nm, Rq 12 nm) for different SRR. The legend in the figure represent different SRR values as percentage sliding.

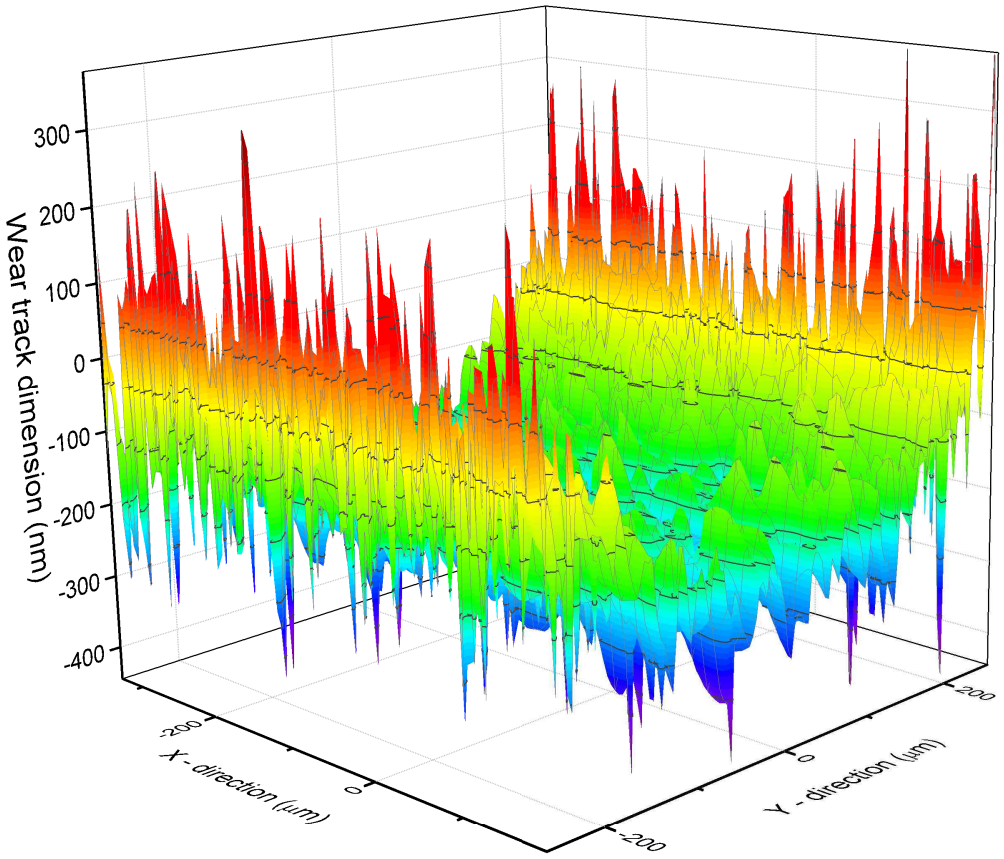

Figure 10: 3-D profile of wear track on the disc simulated by the current model. SRR = +0.5%

References

[1] H. P. Nixon and H. Zantopulos. Lubricant additives, friend or foe: what the equipment design engineer needs to know. *Lubrication engineering*, 51(10), 1995.

[2] H. A. Spikes. The history and mechanisms of zddp. *Tribology letters*, 17(3):469–489, 2004.

[3] M. A. Nicholls, T. Do, P. R. Norton, M. Kasrai, and G. M. Bancroft. Review of the lubrication of metallic surfaces by zinc dialkyldithiophosphates. *Tribology International*, 38(1):15–39, 2005.

[4] P. Studt. Boundary lubrication: adsorption of oil additives on steel and ceramic surfaces and its influence on friction and wear. *Tribology international*, 22(2):111–119, 1989.

[5] A. Morina and A. Neville. Tribofilms: aspects of formation, stability and removal. *Journal of Physics D: Applied Physics*, 40(18):5476, 2007.

[6] M. B. Dobrica and M. Fillon. *Mixed Lubrication*, pages 2284–2291. Springer US, Boston, MA, 2013.

[7] H. A. Spikes and A. V. Olver. Basics of mixed lubrication. *Lubrication science*, 16(1):1–28, 2003.

[8] N. Patir and H. S. Cheng. An average flow model for determining effects of three-dimensional roughness on partial hydrodynamic lubrication. *Journal of lubrication Technology*, 100(1):12–17, 1978.

[9] D. Zhu and H. S. Cheng. Effect of surface roughness on the point contact ehl. *Journal of Tribology*, 110(1):32–37, 1988.

[10] J. A. Greenwood and J. H. Tripp. The contact of two nominally flat rough surfaces. *Proceedings of the institution of mechanical engineers*, 185(1):625–633, 1970.

[11] X. Jiang, D. Y. Hua, H. S. Cheng, X. Ai, and S. C. Lee. A mixed elastohydrodynamic lubrication model with asperity contact. *Journal of tribology*, 121(3):481–491, 1999.

[12] Y. Hu and D. Zhu. A full numerical solution to the mixed lubrication in point contacts. *ASME J. Tribol*, 122(1):1–9, 2000.

[13] J. M. Martin. Antiwear mechanisms of zinc dithiophosphate: a chemical hardness approach. *Tribology letters*, 6(1):1–8, 1999.

[14] J. M. Martin, C. Grossiord, T. Le Mogne, S. Bec, and A. Tonck. The two-layer structure of zndtp tribofilms: Part i: Aes, xps and xanes analyses. *Tribology international*, 34(8):523–530, 2001.

[15] E. Liu and S. D. Kouame. An xps study on the composition of zinc dialkyl dithiophosphate tribofilms and their effect on camshaft lobe wear. *Tribology Transactions*, 57(1):18–27, 2014.

[16] H. Fujita and H. A. Spikes. The formation of zinc dithiophosphate antiwear films. *Proceedings of the Institution of Mechanical Engineers, Part J: Journal of Engineering Tribology*, 218(4):265–278, 2004.

[17] H. Fujita, R. P. Glovnea, and H. A. Spikes. Study of zinc dialkydithiophosphate antiwear film formation and removal processes, part i: experimental. *Tribology transactions*, 48(4):558–566, 2005.

[18] G. M. Bancroft, M. Kasrai, M. Fuller, Z. Yin, K. Fyfe, and K. H. Tan. Mechanisms of tribochemical film formation: stabilityof tribo-and thermally-generated zddp films. *Tribology Letters*, 3(1):47–51, 1997.

[19] M. L. Suominen Fuller, K. L. De Jong, M. Kasrai, and G. M. Bancroft. Electroless generation of phosphate films on metals from zinc dialkyldithiophosphates. *Chemistry of materials*, 12(5):1300–1304, 2000.

[20] B. Mingwu, Z. Xushou, and Qi Shangkui. Tribological properties of silicon nitride ceramics coated with molybdenum films under boundary lubrication. *Wear*, 169(2):181–187, 1993.

[21] N. N. Gosvami, J. A. Bares, F. Mangolini, A. R. Konicek, D. G. Yablon, and R. W. Carpick. Mechanisms of antiwear tribofilm growth revealed in situ by single-asperity sliding contacts. *Science*, 348(6230):102–106, 2015.

[22] T. Haque, A. Morina, A. Neville, R. Kapadia, and S. Arrowsmith. Study of the zddp antiwear tribofilm formed on the dlc coating using afm and xps techniques. *Journal of ASTM International*, 4(7):1–11, 2007.

[23] K. Topolovec-Miklozic, T. R. Forbus, and H. A. Spikes. Film thickness and roughness of zddp antiwear films. *Tribology Letters*, 26(2):161–171, 2007.

[24] J. Zhang and H. A. Spikes. On the mechanism of zddp antiwear film formation. *Tribology Letters*, 63(2):1–15, 2016.

[25] Z. Yin, M. Kasrai, M. Fuller, G. M. Bancroft, K. Fyfe, and K. H. Tan. Application of soft x-ray absorption spectroscopy in chemical characterization of antiwear films generated by zddp part i: the effects of physical parameters. *Wear*, 202(2):172–191, 1997.

[26] N. J Mosey, M. H. Müser, and T. K. Woo. Molecular mechanisms for the functionality of lubricant additives. *Science*, 307(5715):1612–1615, 2005.

[27] C. K. Kajdas. Importance of the triboemission process for tribochemical reaction. *Tribology International*, 38(3):337–353, 2005.

[28] C. G. Camara, J. V. Escobar, J. R. Hird, and S. J. Putterman. Correlation between nanosecond x-ray flashes and stick–slip friction in peeling tape. *nature*, 455(7216):1089–1092, 2008.

[29] C. Kajdas, R. Tummler, H. von Ardenne, and W. Schwarz. The relevance of negative ion mass spectroscopy to the interpretation of the reaction of metal dialkyldithiophosphates during lubricated rubbing. *ZFI Mitteilungen*, 115:107–112, 1986.

[30] S. L. Craig. Mechanochemistry: a tour of force. *Nature*, 487(7406):176–177, 2012.

[31] H. Spikes and W. Tysoe. On the commonality between theoretical models for fluid and solid friction, wear and tribochemistry. *Tribology Letters*, 59(1):21, 2015.

[32] J. Andersson, R. Larsson, A. Almqvist, M. Grahn, and I. Minami. Semi-deterministic chemo-mechanical model of boundary lubrication. *Faraday discussions*, 156(1):343–360, 2012.

[33] A. Akchurin and R. Bosman. A deterministic stress-activated model for tribo-film growth and wear simulation. *Tribology Letters*, 65(2):59, 2017.

[34] A. Ghanbarzadeh, M. CT Wilson, A. Morina, D. Dowson, and A. Neville. Development of a new mechano-chemical model in boundary lubrication. *Tribology International*, 93:573–582, 2016.

[35] A. Ghanbarzadeh, P. Parsaeian, A. Morina, M. CT Wilson, M. CP van Eijk, I. Nedelcu, D. Dowson, and A. Neville. A semi-deterministic wear

model considering the effect of zinc dialkyl dithiophosphate tribofilm. *Tribology Letters*, 61(1):12, 2016.

[36] V. Brizmer, C. Matta, I. Nedelcu, and G. E. Morales-Espejel. The influence of tribolayer formation on tribological performance of rolling/sliding contacts. *Tribology Letters*, 65(2):57, 2017.

[37] A. Ghanbarzadeh. *Mechano-chemical modelling of boundary lubrication*. PhD thesis, University of Leeds, 2016.

[38] Y. Z. Hu and K. Tonder. Simulation of 3-d random rough surface by 2-d digital filter and fourier analysis. *International Journal of Machine Tools and Manufacture*, 32(1-2):83–90, 1992.

[39] S. Liu, Q. Wang, and G. Liu. A versatile method of discrete convolution and fft (dc-fft) for contact analyses. *Wear*, 243(1):101–111, 2000.

[40] W. Z. Wang, H. Wang, Y. C. Liu, Y. Z. Hu, and D. Zhu. A comparative study of the methods for calculation of surface elastic deformation. *Proceedings of the Institution of Mechanical Engineers, Part J: Journal of Engineering Tribology*, 217(2):145–154, 2003.

[41] C. J. A. Roelands. Correlational aspects of the viscosity-temperature-pressure relationship of lubricating oils. 1966.

[42] D. Dowson and G. R. Higginson. *Elasto-hydrodynamic lubrication: the fundamentals of roller and gear lubrication*, volume 23. Pergamon Press, 1966.

[43] Y. Liu, Q. J. Wang, W. Wang, Y. Hu, and D. Zhu. Effects of differential scheme and mesh density on ehl film thickness in point contacts. *Journal of Tribology*, 128(3):641–653, 2006.

[44] K. L. Johnson. Contact mechanics cambridge univ. *Press, Cambridge*, 1985.

[45] F. Sahlin, R. Larsson, A. Almqvist, P. M. Lugt, and P. Marklund. A mixed lubrication model incorporating measured surface topography. part 1: theory of flow factors. *Proceedings of the Institution of Mechanical Engineers, Part J: Journal of Engineering Tribology*, 224(4):335–351, 2010.

[46] A. Azam, A. Dorgham, A. Morina, A. Neville, and Mark C.T. Wilson. A simple deterministic plastoelastohydrodynamic lubrication (pehl) model in mixed lubrication. *Tribology International*, 131:520–529, 2019.

[47] A. Azam. *Modelling interfacial tribochemistry in the mixed lubrication regime*. PhD thesis, University of Leeds, 2018.

[48] S. B. Bulgarevich, M. V. Boiko, V. I. Kolesnikov, and K. E. Korets. Population of transition states of triboactivated chemical processes. *Journal of Friction and Wear*, 31(4):288–293, 2010.

[49] S. B. Bulgarevich, M. V. Boiko, V. I. Kolesnikov, and V. A. Feizova. Thermodynamic and kinetic analyses of probable chemical reactions in the tribocontact zone and the effect of heavy pressure on evolution of adsorption processes. *Journal of Friction and Wear*, 32(4):301–309, 2011.

[50] L. Chang and Y. R. Jeng. A mathematical model for the mixed lubrication of non-conformable contacts with asperity friction, plastic deformation, flash temperature, and tribo-chemistry. *Journal of Tribology*, 136(2):022301, 2014.

[51] Y. C. Lin and H. So. Limitations on use of zddp as an antiwear additive in boundary lubrication. *Tribology International*, 37(1):25–33, 2004.

[52] A. Morina and A. Neville. Understanding the composition and low friction tribofilm formation/removal in boundary lubrication. *Tribology International*, 40(10):1696–1704, 2007.

[53] S. Bec, A. Tonck, J. M. Georges, R. C. Coy, J. C. Bell, and G. W. Roper. Relationship between mechanical properties and structures of zinc dithiophosphate anti–wear films. In *Proceedings of the Royal Society of London A: Mathematical, Physical and Engineering Sciences*, volume 455, pages 4181–4203. The Royal Society, 1999.

[54] G. Nehme, R. Mourhatch, and P. B. Aswath. Effect of contact load and lubricant volume on the properties of tribofilms formed under boundary lubrication in a fully formulated oil under extreme load conditions. *Wear*, 268(9):1129–1147, 2010.

[55] M. Aktary, M. T. McDermott, and G. A. McAlpine. Morphology and nanomechanical properties of zddp antiwear films as a function of tribological contact time. *Tribology letters*, 12(3):155–162, 2002.

[56] R. Mourhatch and P. B. Aswath. Tribological behavior and nature of tribofilms generated from fluorinated zddp in comparison to zddp under extreme pressure conditionspart ii: morphology and nanoscale properties of tribofilms. *Tribology International*, 44(3):201–210, 2011.

[57] J. Archard. Contact and rubbing of flat surfaces. *Journal of applied physics*, 24(8):981–988, 1953.

[58] C. Minfray, J. M. Martin, M. I. De Barros, T. Le Mogne, R. Kersting, and B. Hagenhoff. Chemistry of zddp tribofilm by tof-sims. *Tribology Letters*, 17(3):351–357, 2004.

[59] R. Bosman and D. J. Schipper. Mild wear maps for boundary lubricated contacts. *Wear*, 280:54–62, 2012.

[60] A. N. Suarez. *The behaviour of antiwear additives in lubricated rolling-sliding contacts*. PhD thesis, Luleå tekniska universitet, 2011.